Zircon U-Pb strain chronometry reveals deep impact-triggered flow

D.E. Moser[1*], W.J. Davis[2], S.M. Reddy[3], R.L. Flemming[1], R.J. Hart[4]

ABSTRACT

Large (>100km) meteorite impact cratering events play important roles in surface and biosphere evolution, however, their potential for widespread ductile modification of the lithosphere has been difficult to assess, due partly to our inability to isotopically age-correlate deep mineral fabrics with surface records. We have integrated benchmark U-Pb zircon dating methods (ID-TIMS, SHRIMP) with new microstructural techniques (EBSD, μXRD) to demonstrate that crystal-plastic deformation can cause rapid out-diffusion of radiogenic Pb and accompanying trace element alteration in crystalline zircon. We have used this phenomenon to directly date fabric in Archean zircons and xenoliths of the lower crust of South Africa at 2023±15 million years, coeval with the 2020±3 million year old Vredefort cratering event at surface, with extent ≥20,000 km^2. Our findings indicate that regional exogenic fabrics, similar to high-temperature tectonic fabrics, exist in ancient crust. Moreover, our results establish that crystal-plastic deformation in the lithosphere can now be directly dated and linked to planetary evolution by zircon U-Pb strain chronometry.

[1*]*corresponding author* Dept. of Earth Sciences, University of Western Ontario, London, ON, Canada N6A 5B7; desmond.moser@uwo.ca, tel: 519-661-4214
[2]Geological Survey of Canada, 601 Booth St., Ottawa, Canada, K1A 0E8
[3]Dept. of Applied Geology, Curtin University of Technology, GPO Box U1987, Perth, WA 6845, Australia
[4]iThemba labs, P. Bag 11 Wits 2050, Johannesburg, South Africa

1. Introduction

The rebound and isostatic recovery of multi-kilometer deep impact craters, more prevalent on the early Earth, can potentially generate permanent strain in the deep lithosphere (Ivanov, 2005; Nimmo et al., 2008). The nature of any resulting strain fabrics, however, remains poorly understood due partly to a rarity of samples to test the concept, but also because accurate, direct age correlation of fabrics to impact or short-lived, tectonic events has proved intractable to isotopic dating techniques, including the benchmark zircon U-Pb method. The integrity of zircon as a geochemical capsule preserving primary isotopic and trace element information, unaffected by deformation, is fundamental to the accurate measurement of events in geologic and planetary evolution (e.g. Holmes, 1911; Wilde et al., 2001; Srinivasan et al., 2007). In the continental crust, experimental data demonstrate that thermally-controlled volume diffusion alone should not affect the chemistry of non-metamict zircon particularly in the plastically deforming middle and lower crust where ambient temperatures above ~150ºC prompt rapid repair of alpha- decay lattice damage (Meldrum et al., 1998). Crustal strain-induced Pb diffusion and associated isotopic age re-setting and "discordance" (Wetherill, 1956) in zircon has been proposed (Wayne and Sinha, 1988) but has not yet been demonstrated due to partially metamict samples or possibly because research (e.g. Ashwal et al., 1999) predated advances in microstructural analysis of crystal-plastic zircon deformation (Reddy et al., 2006; Reddy et al., 2007). Here we apply advanced microstructural analysis along with high spatial and isotopic resolution U-Pb zircon dating to mylonitized lower crustal xenoliths from beneath the Witwatersrand basin of South Africa to determine the age and origin of their mineral fabrics.

1.1. Geological Context

The lower crustal xenoliths were recovered from the Lace kimberlite pipe that intruded at 0.132 Ga (Phillips et al., 1998), 60 km from the present geographic center of the deeply eroded Vredfort impact basin in the eastern Kaapvaal craton (Fig. 1). The craton is a remnant of thick, diamondiferous Mesoarchean (3.5 to 3.1 Ga) lithosphere that was coherent by 3.08 Ga (Moser et al., 2001) after which its western margin experienced 2.9 Ga orogenesis followed by 2.7Ga Ventersdorp continental rifting and coeval ultra high-temperature metamorphism of the lower crust (Schmitz and Bowring, 2003). Structural modification, impact melting and local metamorphism of the basement to the gold-rich upper crust occurred at 2.020±.003 Ga as a result of the Vredefort impact (Spray et al., 1995; Moser, 1997) that formed a crater with a final diameter of ~250 km and maximum depth of excavation of ~10 km (Henkel and Reimold, 1998). Shock pressures experienced by the base of the >38 km Kaapvaal crust (Nguuri et al., 2001) beneath the Lace pipe would have been less than the 20 GPa threshold for shock deformation of zircon (Leroux et al., 1999) due to shock wave attenuation of ~4 GPa/km over the radial distance of ~80 km from the original point of impact (Gibson and Reimold, 2005). Microstructural features indicative of shock metamorphism have not been reported in zircon or main phase assemblages in previous petrologic investigations of the Lace lower crustal xenolith suites (Dawson et al., 1997; Schmitz and Bowring, 2003). Shock wave heating is also predicted to have been insignificant at this region of the crust (Henkel and Reimold, 2002) where, after decay of the Ventersdorp thermal pulse, ambient temperatures cooled from 650°C to 350°C (Gibson and Jones, 2002), i.e., consistently above the self-annealing temperature of zircon radiation damage.

2. Methods

High precision, U-Pb isotope geochronology was performed first by applying isotope dilution thermal ionization mass spectrometry (ID-TIMS) on air-abraded single zircons or CL-imaged zircon fragments at the Jack Satterly Geochronology Laboratory, Royal Ontario Museum/University of Toronto using methods described in Moser and Heaman (1997). Details of analytical corrections and U-Pb isotopic spike are provided in Table 1. Zircon internal structure and lattice orientation in thin sections and polished grain mounts were measured at the University of Western Ontario using colour SEM-Cathodoluminescence (SEM-CL) and a microbeam (50 µm diameter) X-ray diffractometer (µXRD)(Flemming, 2007). SIMS spot analyses of U-Th-Pb isotopes and trace elements at the Geological Survey of Canada SHRIMPII laboratory were performed prior to Electron Backscatter Diffraction (EBSD) mapping of the SHRIMPII grain mount at the Curtin University of Technology. Details on analytical protocols and run conditions employed in these techniques are provided as Supplementary Material.

3. Results of zircon analysis

The Lace mafic xenoliths feature a primary assemblage of garnet-clinopyroxene-plagioclase-quartz that is typical of high pressure (0.9 GPa to 1.2 GPa) granulite facies samples of the lower continental crust (Pattison, 2003). These exhibit mylonitic planar fabrics (Fig. S1) commonly produced by high temperature ductile strain (Snoke and Tullis, 1998). Detailed analysis was carried out on five mafic mylonite xenoliths (LG-1,2,3,5 and 6), between 3 and 5 cm in maximum dimension, that feature garnet porphyroclasts in a fine-grained groundmass of anhedral clinopyroxene, plagioclase, garnet, quartz and oxide minerals with trace zircon and apatite (Fig. S1). Xenolith LG2 contained a leucocratic layer (LG2b) that was processed for zircon separation separately from the main mass (LG2a). Zircons occur as inclusions in the garnet porphyroclasts as well as at grain boundaries of mylonitized matrix minerals (Fig. 2) and are optically continuous, light to dark pink, high-luster grains with forms ranging from subhedral long-prismatic to round, highly-embayed anhedra.

3.1. Cathodoluminescence and μXRD

The zircon internal structure revealed by SEM-CL consists of three zones; Type 1 igneous, planar growth-banded cores, Type 2 brightly luminescent, rounded metamorphic rims and Type 3 complexly zoned domains of intermediate CL intensity and indistinct ‘cloudy’ to discontinuous banding occurring at cores and/or rims of grains (Fig. 2). *In situ* μXRD analysis of an elongate Type 1 and 2 zoned zircon within the core of a garnet porphyroclast (LG-6) gives a discrete point reflection pattern for zircon (112) and (431) planes and enclosing garnet plane (312) consistent with undeformed single crystals. Two ovoid zircons near the mylonitized margin of the garnet porphyroclast show distorted core/rim boundaries and nebulous type 3 CL zoning, and yield arcs or streaks of X-ray reflectors indicating strain within the crystal (Flemming, 2007) and a mosaicity of 3 degrees. Neighboring feldspar and clinopyroxene show even greater mosaicity and lattice deformation consistent with undulose extinction patterns apparent in polarized light microscopy. A Type 3 zircon within the mylonitic foliation of xenolith LG-5 yielded a similar μXRD pattern consistent with crystal-plastic deformation.

3.2. U-Pb isotope and trace element composition

Prior to microstructural analysis, single zircons or zircon fragments exhibiting a range of morphology and zoning types were analyzed by ID-TIMS. The results range from concordant to 60% discordant along a discordia line with intercepts at 2670±4 Ma and 2015±18 Ma (MSWD=0.42)(Fig. 3; table 1; all U-Pb data reported at 2σ confidence). The collinearity of the data from the five different xenoliths suggests a common history for the xenolith source region beginning at 2.67 Ga, whereas the high precision of the single grain analyses clearly indicates discordance relating to an episode at 2.02 Ga. To identify the discordant domains within single grains, 64 SHRIMP II analyses were carried out on grains from LG1 (8 grains), LG-2a (14 grains) and LG-2b (7 grains) (Fig. 3; table S1). Type 1 cores and type 2 rims yield ages of 2.67 Ga, plotting at or near the upper concordia intercept determined by ID-TIMS (Fig. 3). The weighted mean $^{207}Pb/^{206}Pb$ age of 2663±7 Ma (MSWD = 0.39), determined from the eight most concordant Type 1 cores, is within error of the weighted mean $^{207}Pb/^{206}Pb$ age of 2654±12 Ma determined for Type 2 rim domains. Trace element measurements of cores and rims by SHRIMPII reveal large changes in U and HREE concentration (table S2). Type 1 cores exhibit high [U] (870 to 1800 ppm, n=4) and elevated HREE abundances typical of igneous zircon (Hoskin and Black, 2000), whereas rims are markedly lower in relative [U], Th/U and HREE.

The Type 3 zones were found to be the source of discordant data with individual analyses plotting from 30% to 100% down the discordia line (Fig. 3). The greatest discordance was measured in Grain 17 of xenolith LG-2A where multi-spot analyses (n= 15) allow contouring of the pattern of discordance in the grain interior (Fig. 4). Discordance is at a minimum at grain edges and increases to maximum values of 100% in a central corridor (Fig. 4). The weighted mean of the 6 youngest $^{207}Pb/^{206}Pb$ ages from the central zone is 2023±15, within error of the ID-TIMS lower intercept age of 2018±15 Ma. Trace element analysis reveals variations in [U] across the grain unrelated to the degree of discordance (fig. S2, table S2). Discordance instead correlates with LREE abundance, with a five-fold relative increase in Ce abundance, and a La/Sm ratios increase from 0.02 to as much as 0.60, in the zone of 100% discordance (fig. S2).

3.3. Zircon crystal-plastic strain and microstructure

Whole-grain strain analysis of Grain 17 by μXRD indicates 2 to 3 degrees of mosaicity of the (112), (321) and (301) planes (Fig. 4) – identical to that measured in Type 3 grains in the mylonitic fabric in thin sections of LG-6 and LG-5. Strain mapping of the Grain 17 surface by EBSD, after re-polishing to remove ~1 micron ion probe pits and following new procedures (Reddy et al. 2007; 2008), reveals pervasive incremental lattice rotation about a central 'shear' defined by a concentration of low angle grain boundaries that coincide with the zone of 100% discordance (Fig. 4). Automatic EBSD mapping illustrates up to 20° of cumulative misorientation across the polished grain surface accommodated by low-angle boundaries (Fig. 4). Dispersion of crystallographic axes around numerous small circles (Fig. 4) suggests that multiple slip systems were operating during intragrain deformation.

4. Zircon U-Pb strain chronometry

Proof of strain-induced U-Pb age discordance in zircon must satisfy several conditions: 1) the zircons must have remained above the radiation damage self-annealing temperature of ~150°C (Meldrum et al., 1998) before and after deformation in order to preclude the possibility that U-Pb age discordance occurred by Pb-loss from radiation-damaged domains; 2) the ductilely deformed (as opposed to recrystallized) zircon domains must be identified *in situ* and shown to be contemporaneous with the deformation fabric in the host rock, and 3) the U-Pb isotopic data must be of sufficient analytical and spatial resolution to demonstrate a correlation of discordance with zircon microstructure. We maintain that our investigation fulfills these requirements and demonstrates a clear case of strain-induced Pb-loss in zircon.

Evidence that the zircons we have analysed were in the deep crust, and therefore non-metamict, during deformation is derived from the zircon data and regional geophysical/ geological constraints. Type 1 oscillatory zoned cores have high U concentrations yet are optically clear and non-metamict in appearance. They yield concordant Archean U-Pb ages by ID-TIMS at 2.670±.004 Ga and SHRIMP at 2.663±.007 Ga. Based on the oscillatory zoning structure of the cores, and the extremely sluggish diffusion of Pb in undeformed, lower crustal zircon during metamorphism (e.g. Moser et al., 2008), these values are interpreted to date the crystallization of the igneous mafic protoliths in the deep crust. The protoliths are seen as deep-seated counterparts to voluminous surface eruption of 2.664±.002 Ga Pneil-stage flood basalts (Barton et al., 1995) late in the Ventersdorp rifting on the western margin of the craton. Evidence for cooling and autometamorphism of the intrusions to form the present garnet granulite facies assemblage is indicated by the dramatic decrease in the abundance of HREE (e.g. Rubatto, 2002) in coeval 2.66 Ga Type 2 zircon rims. This petrogenetic evidence for an intrusive mafic intraplate at the base of the crust is in concert with the sharp increase in seismic wave velocities observed at the Moho of the eastern Kaapvaal craton (Nguuri et al., 2001). Together with the zircon crystallization history, these data are consistent with residence and deformation of these samples in the lower crust at temperatures in excess of the annealing temperature of zircon radiation damage.

The timing relationship between zircon deformation and mylonitization of the host is shown by the *in situ* μXRD and colour SEM-CL measurements of thin section LG-6. Zircon and host garnet at the center of a porphyroclast are undeformed, the zircon having been armoured by garnet, whereas zircons in the mylonitized edges of the same garnet show clear evidence of crystal-plastic strain (Fig. 2). This spatial association of strained zircon with the petrofabric is critical as it allows us to correlate the timing of zircon deformation to the deformation of the host mineral assemblage. The μXRD data for deformed zircons *in situ* (Fig. 3) and for separated Grain 17 (Fig. 4) are identical, and permit mapping of *in situ* zircon/petrofabric strain and relative time relationships to the microstructural and absolute age data for Grain 17.

A comparison of the lattice strain and isotopic data for Grain 17 reveals the critical link between age discordance and microstructure. The μXRD pattern for the entire grain shows short arcs from lattice plane reflectors indicating low angle grain boundaries as opposed to discrete point reflections from a polycrystalline aggregate produced by recrystallization. The EBSD data confirm this and show that low angle boundaries, developed by dislocation creep, define a microstructure that correlates spatially with the central zone of isotopic resetting (Fig. 4). The low variation of [U] across this zone, and the lack of correlation between [U] and discordance in Grain 17 (fig. S3, table S1), indicate that discordance is due to Pb-loss rather than U-gain. Based on this spatial correlation of Pb-loss and structure, the low angle grain boundaries are interpreted to mark the location of high diffusivity pathways that facilitated relatively rapid out-diffusion of Pb during a ductile flow and mylonite fabric forming event. The detailed mechanisms of fast diffusion are the subject of current investigation, however the relative enrichment of La, Ce and LREE proportional to discordance in Grain 17 (fig. S2, table S2) suggests that diffusion involved participation of a fluid that produced trace element enrichment similar to that reported in domains of crystal-plastic zircon in the lower oceanic crust (Reddy et al., 2006).

5. Implications for planetary processes and chronology

Having established that discordance is caused by lattice strain, and that zircon strain is contemporaneous with mylonitization of the host mineral assemblage, the U-Pb discordia line can be used to construct a first zircon strain chronometry of the lithosphere. In this case the 2.02±0.02 Ga lower intercept of the ID-TIMS discordia line, and the 2.02±0.02 Ga average $^{207}Pb/^{206}Pb$ age of SHRIMP spots (n=7) for the shear zone at the center of Grain 17, can be interpreted as dating mylonitization of the xenolith samples. As this deformation age is at a time of quiescence in the Kaapvaal craton, and agrees with the 2.020+/-.003 Ga formation of the Vredefort impact basin, mylonite formation is interpreted to be related to impact basin dynamics. Geophysical profiling of the Vredefort impact basin indicates a gentle upward rotation of seismic reflectors at the crust-mantle transition at a geographic distance of 60 km from center of impact (Durrheim et al., 1991), approximately the same radial distance as the piercing point of the Lace kimberlite pipe (Fig. 5). It has been suggested that tilting of these reflectors could be the result of plastic deformation during crater rebound and return flow (Henkel and Reimold, 1998).

Our findings are in concert with this interpretation noting that the kms^{-1} crustal motions induced by the initial depression and rebound of the transient crater would have been too great to have been accommodated by mylonite formation in the lower crust. We propose that the fabric we have dated formed in shear zones at the base of the crust during the relatively longer-term recovery of the lithosphere that accompanied post-impact modification and isostatic re-equilibration of the multi-kilometer deep crater. Impact processes are generally radially symmetric and lower crustal mylonitization should have a geographic distribution beneath the crater at least to the distance of the Lace kimberlite. If so, the fabric would extend over ≥20,000 km^2 of the South African crust-mantle transition. The LREE enrichment of ductile deformed zircon in our sample suggests fluid participation in mylonitization, and such regional flow of the deep crust and related fluid channeling following impact may have played a role in driving the minor remobilization of gold in the overlying deposits of the Witwatersrand basin (Hayward et al., 2005).

Our investigation of continental lower crust, and earlier work on oceanic lower crust (Reddy et al., 2006), indicates that ductile deformation of zircon occurs in mafic and/or garnet-bearing lithosphere, and the discovery that this strain can induce minor to complete U-Pb zircon age discordance merits awareness and exploitation. Strain-induced discordance in zircon may explain some low levels of discordance, discordant arrays, or 'smears' of U-Pb data along concordia commonly observed in metamorphic rocks (e.g. Ashwal et al., 1999; Harley et al., 2007). On the other hand it should be noted that pronounced strain-induced discordance is exhibited by the minority of zircons in our samples, and these exhibit distinctive CL zoning. Targeting such grains opens the door to the direct dating of lithospheric flow with a corresponding accuracy that has so far eluded geochronology. Regarding the robustness of the zircon strain record, our results are encouraging as they indicate that low-angle boundaries and associated age disturbance in zircon have persisted at ambient lower crustal temperatures for almost 2 billion years. The abundance of such zones of ductile deformation-altered zircon within the thousands of metamorphic and detrital zircon populations analyzed for geochronology over the last several decades remains to be seen.

Our results emphasize that understanding the microstructural state of minerals is important for the correct interpretation of isotopic and trace element data of mineral geochronometers in deformed assemblages and extraterrestrial phases (e.g., Srinivasan et al., 2007; Pidgeon et al., 2007). A more immediate implication is that impact processes can now be considered when interpreting ductile fabric genesis, particularly in ancient, high grade metamorphic terrains where such fabrics are common and surface evidence of large impacts has been lost to erosion. It is hoped that further investigations of the type we have carried out will foster direct measurement of the strain history of the lithosphere of Earth and perhaps other rocky planets, and improve the accuracy of planetary chronologies upon consideration of this new mechanism for generating discordance in zircon.

Acknowledgments

Support from Prof. T.E. Krogh and Prof. D.J. Schulze (University of Toronto) in launching this research is gratefully acknowledged, as is a National Science and Engineering Research Council Discovery Grant to DEM. Dr. Dazhi Jiang (University of Western Ontario) is thanked for helpful discussions regarding mylonites. Expert drafting was contributed by Patricia Connor (UWO Dept. of Geography). Australian Research Council Discovery Grant DP0664078 and a Curtin University Targeted Research Fellowship to SMR are gratefully acknowledged.

REFERENCES

Ashwal, L.D., Tucker, R.D., Zinner, E.K., 1999. Slow cooling of deep crustal granulites and Pb-loss in zircon. *Geochimica et Cosmochimica Acta,* **63**, 2839–2851.

Barton Jr., J.M., Blignault, E., 1995. A review of the geochronological constraints on the evolution of the Kaapvaal Craton, South Africa. *South African Journal of Geology* **98**, 386-392.

Dawson, J.B., Harley, S.L., Rudnick, R.L., Ireland, T.R., 1997. Equilibration and reaction in Archaean quartz-sapphirine granulite xenoliths from the Lace kimberlite pipe, South Africa. *Journal of Metamorphic Geology* **15**, 253–266.

Durrheim, R.J., Nicolaysen, L.O., Corner, B., 1991. A deep seismic reflection profile across the Archean – Proterozoic Witwatersrand basin, South Africa. Continental Lithosphere: Deep Seismic Reflections. AGU Geodyn. Ser., vol. 22, pp. 213–224.

Flemming, R.L., 2007. Micro X-ray diffraction (μXRD): a versatile technique for characterization of Earth and planetary materials. *Canadian Journal of Earth Sciences* **44**, 1333-1346.

Gibson, R.L., Jones, M.Q.W., 2002. Late Archean to Palaeoproterozoic geotherms in the Kaapvaal craton: constraints on the thermal evolution of the Witwatersrand Basin. *Basin Research* **14**, 169-181.

Gibson, R.L., Reimold, W.U., 2005. Shock pressure distribution in the Vredefort impact structure, South Africa. *Geol. Soc. Amer. Spec. Pap*. **384**, 329-349.

Harley, S.L., Kelly, N.M., Moeller, A., 2007. Zircon behaviour and the thermal histories of mountain chains. *Elements* **3**, 25-30.

Hayward, C.L., Reimold, W.U., 2005. Gold mineralization within the Witwatersrand Basin, South Africa: evidence for a modified placer origin, and the role of the Vredefort impact event. *Geol. Soc. London, Special Publications* **248**, 31-58.

Henkel, H., and Reimold, U.W., 1998. Integrated geophysical modelling of a giant, complex impact structure: anatomy of the Vredefort Structure, South Africa. *Tectonophysics* **287**.

Henkel, H., and Reimold, U.W., 2002. Magnetic model of the central uplift of the Vredefort impact structure, South Africa. *Journal of Applied Geophysics* **51**, 43-62.

Holmes, A., 1911. The association of lead and uranium in rock-minerals, and its application to the measurement of geologic time. *Proc. Royal Society (London)* **85A,** 248-256.

Hoskin, P.W.O., Black, L.P., 2000. *Journal of Metamorphic Geology* **18**, 423-439 (2000).

Ivanov, B.A., 2005. Numerical modeling of the largest terrestrial meteorite craters. *Solar Syst. Res.* **39**, 381-409.

Leroux, H., Reimold, W.U., 1999. Experimental shock deformation in zircon: a transmission electron microscopic study. *Earth Planet. Sci. Lett.* **169**, 291-301.

Meldrum, L.A., Boatner, W.J., Weber, J., Ewing, R.C., 1998. Radiation damage in zircon and monazite. *Geochimica et Cosmochimica Acta* **62**, 2509–2520.

Moser, D.E., 1997. Dating the shock wave and thermal imprint of the giant Vredefort impact, South Africa. *Geology* **25**, 7-10.

Moser, D.E. and Heaman, L.M., 1997. Proterozoic zircon growth in Archean lower-crustal xenoliths, southern Superior craton – a consequence of Matachewan ocean opening, *Contributions to Mineralogy and Petrology*, 128: 164-175.

Moser, D.E., R. Flowers, R., Hart, R.J., 2001. Birth of the Kaapvaal tectosphere 3.08 billion years ago. *Science* **291**, 465-468.

Moser, D.E., Bowman, J.R., Wooden, J., Mazdab, F., Valley, J.W., Kita, N, 2008. Creation of a continent recorded in zircon zoning. *Geology*, **36,** 239-242.

Nguuri, T.K., Gore, J., 2001. Crustal structure beneath southern Africa and its implications for the formation and evolution of the Kaapvaal and Zimbabwe cratons. *Geophys. Res. Lett.* **28**, 2501-2504.

Nimmo, F., Hart, S.D., Korycansky, D.G., Agnor, C.B., 2008. Implications of an impact origin for the martian hemispheric dichotomy, *Nature* **453,** 1220-1223.

Pattison, D.R.M., 2003. Petrogenetic significance of orthopyroxene-free garnet+ clinopyroxene+plagioclase + or - quartz-bearing metabasites with respect to the amphibolite and granulite facies. *Journal of Metamorphic Geology* **21**, 21-34.

Phillips, D., Machin, K.J., Kiviets, G.B., Fourie, L.F., Roberts, M.A., Skinner, E.M.W., 1998. A petrographic and $^{40}Ar/^{39}Ar$ geochronological study of the Voorspoed kimberlite, South Africa: Implications for the origin of Group II kimberlite magmatism. *South African Journal of Geology* **101**, 299-306.

Pidgeon, R.T., Nemchin, A.A., van Bronswijk, W., Geisler, T., Meyer, C., Compston, W., Williams, I.S., 2007. Complex history of a zircon aggregate from lunar breccia 73235. *Geochimica et Cosmochimica Acta* **71**, 1370–1381.

Reddy, S.M., N.E. Timms, N.E., Buchan, C., Trimby, P., Blake, K., 2006. Crystal-plastic deformation of zircon: A defect in the assumption of chemical robustness. *Geology* **34**, 257-260.

Reddy, S.M., Timms, N.E., Pantleon, W., Trimby, P., 2007. Quantitative characterization of plastic deformation of zircon and geological implications. *Contributions to Mineralogy and Petrology* **153**, 625-645.

Reddy, S.M., Timms, N.E., 2008. Electron backscatter diffraction analysis of zircon: A systematic assessment of match unit characteristics and pattern indexing optimization. *American Mineralogist*, **93**, 187-197.

Rubatto, D., 2002. Zircon trace element geochemistry: partitioning with garnet and the link between U-Pb ages and metamorphism. *Chemical Geology* **184**, p.123-138.

Schmitz, M.D., Bowring, S.A., 2003. Ultrahigh-temperature metamorphism in the lower crust during Neoarchean Ventersdorp rifting and magmatism, Kaapvaal Craton, southern Africa. *Geol. Soc. Amer. Bull.* **115**, 533-548.

Snoke, A.W., Tullis, J., 1998. in *Fault-related Rocks-a Photographic Atlas*, A.W. Snoke, J. Tullis, Eds. (Todd, Princeton, N.J).

Spray, J.G. , Kelley, S.P. and Reimold, W.U. 1995. Laser-probe $^{40}Ar/^{39}Ar$ dating of coesite- and stishovite-bearing pseudotachylytes and the age of the Vredefort impact event. *Meteoritics* **30**, 335-343.

Srinivasan, G., M. J. Whitehouse, M.J., Weber, I., Yamaguchi, A., 2007. The crystallization age of eucrite zircon. *Science* **317**, 345-347.

Stacey, J.S. and Kramers, J.D., 1975. Approximation of terrestrial lead isotope evolution by a two-stage model. *Earth and Planetary Science Letters* **26**, 207-221.

Wayne, D.M., Sinha, A.K., 1988. Physical and chemical response of zircons to deformation. *Contrib Mineral Petrol* **98**, 109-121.

Wetherill, G.S., 1956. An interpretation of the Rhodesia and Witwaterstrand age patterns. *Geochim Cosmochim Acta* **9** : 290-292.

Wilde, S.A., Valley, J.W., Peck, W.H., Graham, C.M., 2001. Evidence from detrital zircons for the existence of continental crust and oceans on the Earth 4.4 Gyr ago. *Nature* **409**, 175-178.

Supplementary Material

Methods

Figs. S1, S2, S3

Tables. S1, S2, S3

Figure Legends

Figure 1: Basement geology map of the Kaapvaal craton showing the central uplift of the 2.020 Ga Vredefort impact basin, and the location of the 0.132 Ga Lace kimberlite pipe from which the mafic granulite xenoliths were collected. Dashed ring represents former trace of the ~250 km-diameter crater on the now deeply eroded craton.

Figure 2: SEM backscatter electron (BSE) image of thin section of xenolith LG-6 showing; A, zircon included in garnet porphyroclast, and; B and C, zircons at garnet edge within the enveloping mylonitic fabric. Magnified CL images show type 1 (igneous, garnet-absent) cores and type 2 (recrystallized, garnet present) rims; both of which are interpreted to have remained undeformed (see μXRD point pattern) since 2.67 Ga. Zircons in the mylonitic grain fabric show more complex type 3 zoning and crystal-plastic strain (note arc-shaped lattice plane reflections in μXRD patterns).

Figure 3: U-Pb Concordia plots showing results of ID-TIMS dating of single zircons from all xenoliths (above) and SHRIMPII dating of xenoliths LG1, LG2 (below). The data demonstrate variable Pb-loss from original 2.67 Ga zircon along a discordia line to 2.02 Ga. The high isotopic resolution ID-TIMS demonstrates clearly that data lie beneath concordia and are discordant. The high spatial resolution SHRIMPII dating permits correlation of discordance with specific zircon domains identified by CL, and microstructural analysis. Only by combining the complimentary strengths of these techniques can we demonstrate a strain-induced discordance event that overlaps the time of Vredefort impact basin dynamics at 2020±3 Ma.

Figure 4: TOP; grayscale SEM-CL image of polished zircon LG-2a Grain 17 showing ion probe pits and corresponding $^{207}Pb/^{206}Pb$ model ages. Degree of Pb- loss experience by each ion pit volume was calculated based on position on chord between 2.670 Ga and 2.020 Ga. MIDDLE: Orientation contrast image of same grain, following removal of ion probe pits, generated with EBSD and indicating relative concentration of low angle grain boundaries in central corridor. Superposition of Pb-loss contours indicates a spatial correlation between central N-S trending, corridor of subgrain boundaries with a zone of complete U-Pb isotopic resetting of the U-Pb system at 2.02 Ga. The youngest $^{207}Pb/^{206}Pb$ ages (n=6) from this microstructure are interpreted to directly date crystal-plastic deformation. MIDDLE inset: A µXRD pattern of Grain 17 following ion probe analysis. Note short arcs on zircon (112) and (321) lattice planes indicating bulk crystal plastic strain of the grain with a mosaicity of 3 degrees identical to deformed zircons in mylonitic zones in thin section LG-6 (Note that faint ring patterns are due to clay in paper masking neighbouring zircons on SHRIMP mount). BOTTOM: EBSD measurements of lattice rotation and stereonet projection of poles to lattice planes indicating distortion accommodated by multiple slip systems.

Figure 5: Schematic, cross-sectional view of thermal, pressure and motion fields beneath the central zone of the Vredefort impact basin (modified after Henkel and Reimold (1998; 2002) at time of impact at 2020 ±3 Ma indicating the location of the 132 Ma Lace kimberlite pipe and the source region of the mafic mylonite xenoliths containing the ductile zircon analyzed in our study. The impact-generated mylonitic fabrics formed at

the same distance from impact center as gently upturned seismic reflectors in the crust-mantle transition reported by Durrheim et al. (1991) and may represent post-impact ductile flow across the region during recovery of the multi-kilometer deep crater.

Table
Click here to download Table: Moser et al IDTIMS Table 1.pdf

TABLE S1. ID-TIMS U-Pb data

Fraction number/ description [a])	Weight [μg]	U[b]) [ppm]	Pb_{com}[c]) [pg]	Th/U[d])	$^{206}Pb/^{204}Pb$[e])	$^{206}Pb/^{238}U$[f])	$^{207}Pb/^{235}U$[f])	$^{207}Pb/^{206}Pb$[f])	$^{207}Pb/^{206}Pb$[f]) [Ma] (%disc)
Xenolith LG1									
LG1-Z3	2	470	1.3	0.49	18 921	0.4193 ±14	8.660 ±30	0.14978 ±18	2343±2 (4.3%)
LG1-4--ZB	2	650	1.4	0.57	26 601	0.4391 ±10	9.498 ±22	0.15690 ±18	2423±2 (3.8%)
LG1-4--ZC	4	540	2.3	0.67	28 670	0.4673 ±10	11.212 ±28	0.17073 ±20	2565±2 (2.5%)
LG1-5-ZE	3	480	2.3	0.41	18 893	0.4805 ±12	11.423 ±30	0.17241 ±26	2581±3 (2.4%)
Xenolith LG2									
LG2A-1ZA	1	630	1.2	0.55	30 701	0.4845 ±12	11.574 ±30	0.17328 ±22	2590±2 (2.0%)
LG2B-1ZA	2	1460	1.4	0.50	65 501	0.4930 ±10	12.005 ±28	0.17660 ±16	2621±2 (1.7%)
LG2B-1ZC	2	1180	1.6	0.51	47 550	0.5041 ±10	12.462 ±30	0.17928 ±16	2646±1 (0.7%)
Xenolith LG3									
LG3-Z1	4	270	2.5	0.54	13 340	0.4982 ±14	12.150 ±32	0.17686 ±28	2624±3 (0.8%)
Xenolith LG5									
LG5-Z1	2.5	210	0.6	0.49	29 317	0.4907 ±12	11.839 ±30	0.17498 ±18	2606±2 (1.5%)
LG5-Z2	4	200	0.8	0.45	58 193	0.4559 ±14	10.289 ±30	0.16367 ±28	2894±3 (3.5%)
Xenolith LG6									
LG6-Z1	1	530	0.7	0.46	25 940	0.5072 ±12	12.573 ±32	0.17980 ±20	2651±2 (0.3%)
LG6-Z2	1	200	1.0	0.48	6 611	0.5082 ±16	12.632 ±42	0.18026 ±24	2655±2 (0.3%)

[a]) Unless otherwise stated all the zircons are clear, transparent grains, from least paramagnetic fractions of Frantz separates, free of cracks and inclusions. In this case all are single grain, or grain-fragment, analyses.

[b]) U concentrations known to better than 5 % for sample weights over 50 μg and about 50% for sample weights below 2 μg.

[c]) Total common Pb (corrected for fractionation and spike); assigned to blank and subtracted from total Pb for age calculations.

[d]) Model Th/U inferred from $^{208}Pb/^{206}Pb$ using the $^{207}Pb/^{206}Pb$ age.

[e]) corrected for fractionation and spike.

[f]) corrected for fractionation, spike, blank Pb, and initial common Pb if total common Pb > 5pg. Initial Pb composition estimated using Stacey and Kramers (1975) model. Uncertainty estimated with error propagation procedure that accounts for measurement errors, blank uncertainties and reproducibility of Pb and U standards and the effect of an uncertainty of ±2% on the initial Pb composition and 1% on the blank Pb composition. Uncertainties on ratios and ages are quoted at 2 sigma level of confidence.

Figure 1

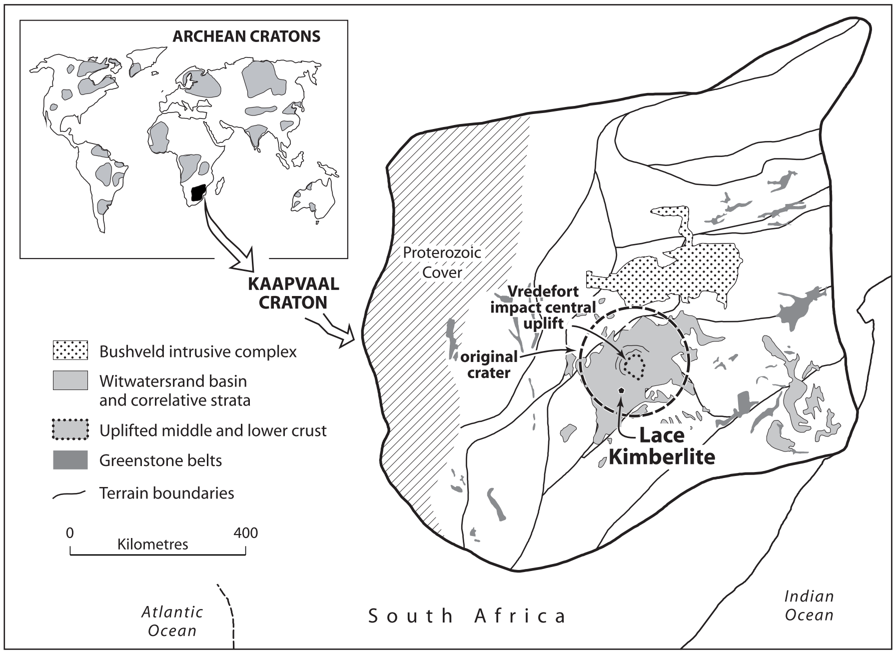

ARCHEAN CRATONS
KAAPVAAL CRATON
Proterozoic Cover
Vredefort impact central uplift
original crater
Lace Kimberlite
Bushveld intrusive complex
Witwatersrand basin and correlative strata
Uplifted middle and lower crust
Greenstone belts
Terrain boundaries
0
400
Kilometres
Atlantic Ocean
South Africa
Indian Ocean

Figure 2

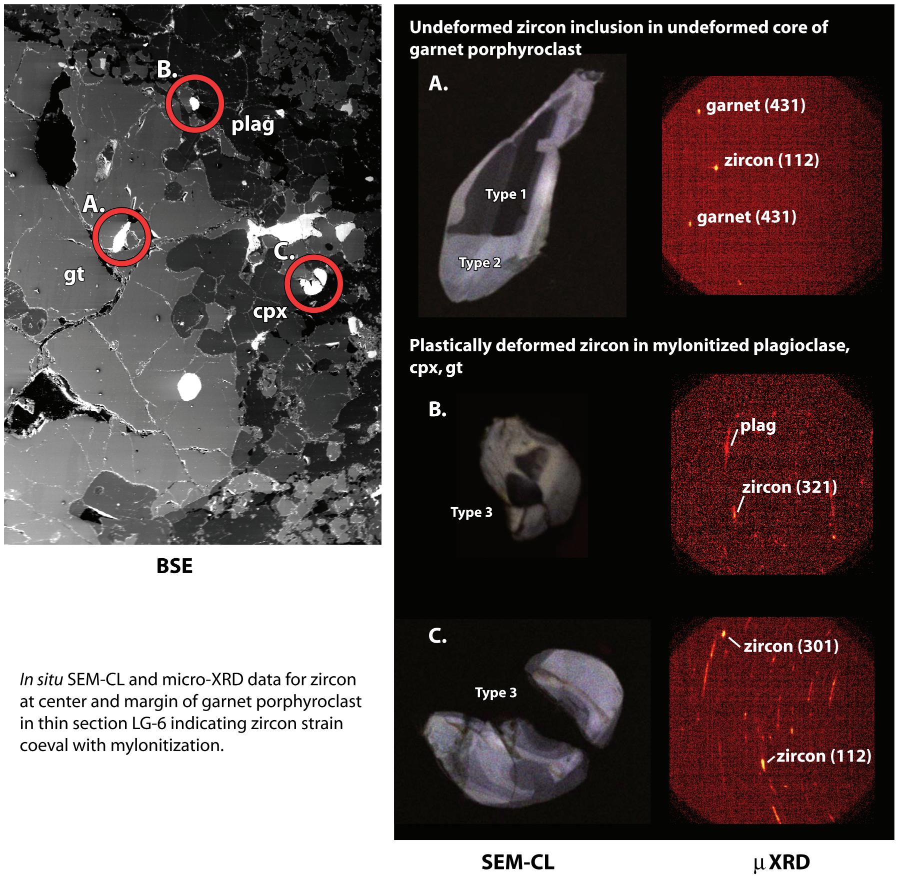

In situ SEM-CL and micro-XRD data for zircon at center and margin of garnet porphyroclast in thin section LG-6 indicating zircon strain coeval with mylonitization.

Figure 3

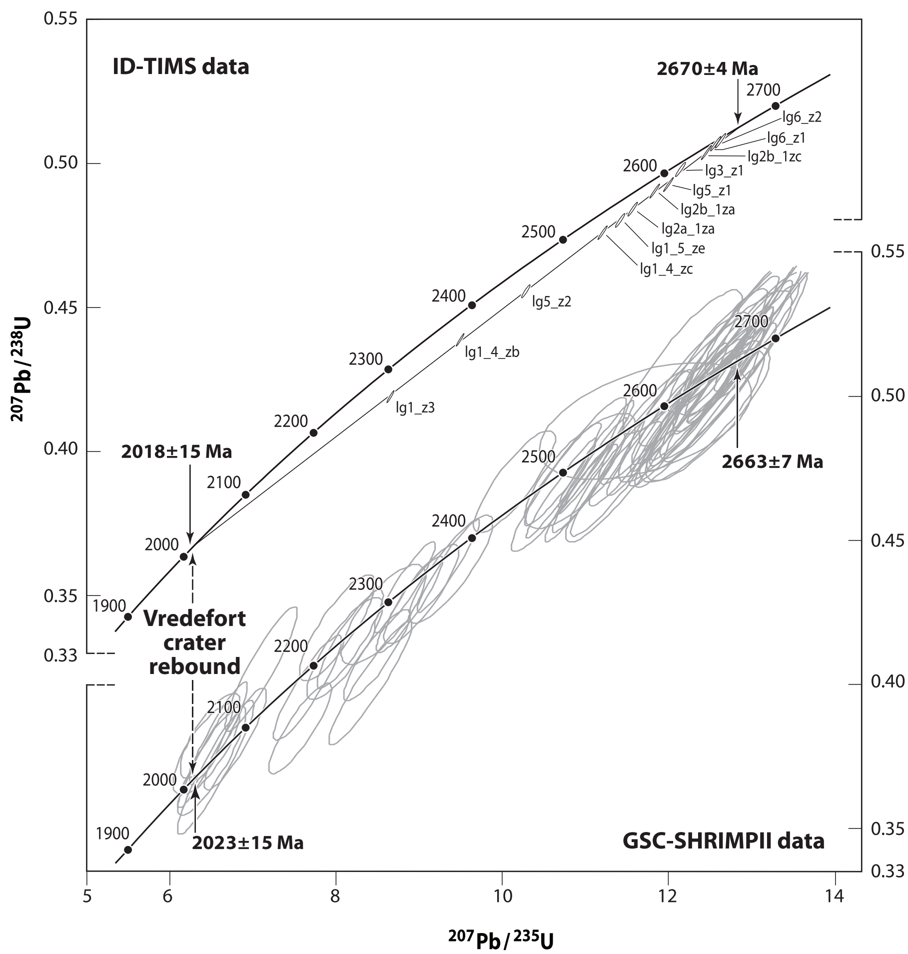

ID-TIMS data
2670±4 Ma
2700
lg6_z2
lg6_z1
lg2b_1zc
lg3_z1
lg5_z1
lg2b_1za
lg2a_1za
lg1_5_ze
lg1_4_zc
lg5_z2
lg1_4_zb
lg1_z3
2600
2500
2400
2300
2200
2100
2000
1900
2018±15 Ma
Vredefort crater rebound
2663±7 Ma
2023±15 Ma
GSC-SHRIMPII data
0.55
0.50
0.45
0.40
0.35
0.33
5
6
8
10
12
14
$^{207}Pb/^{238}U$
$^{207}Pb/^{235}U$

Figure 4

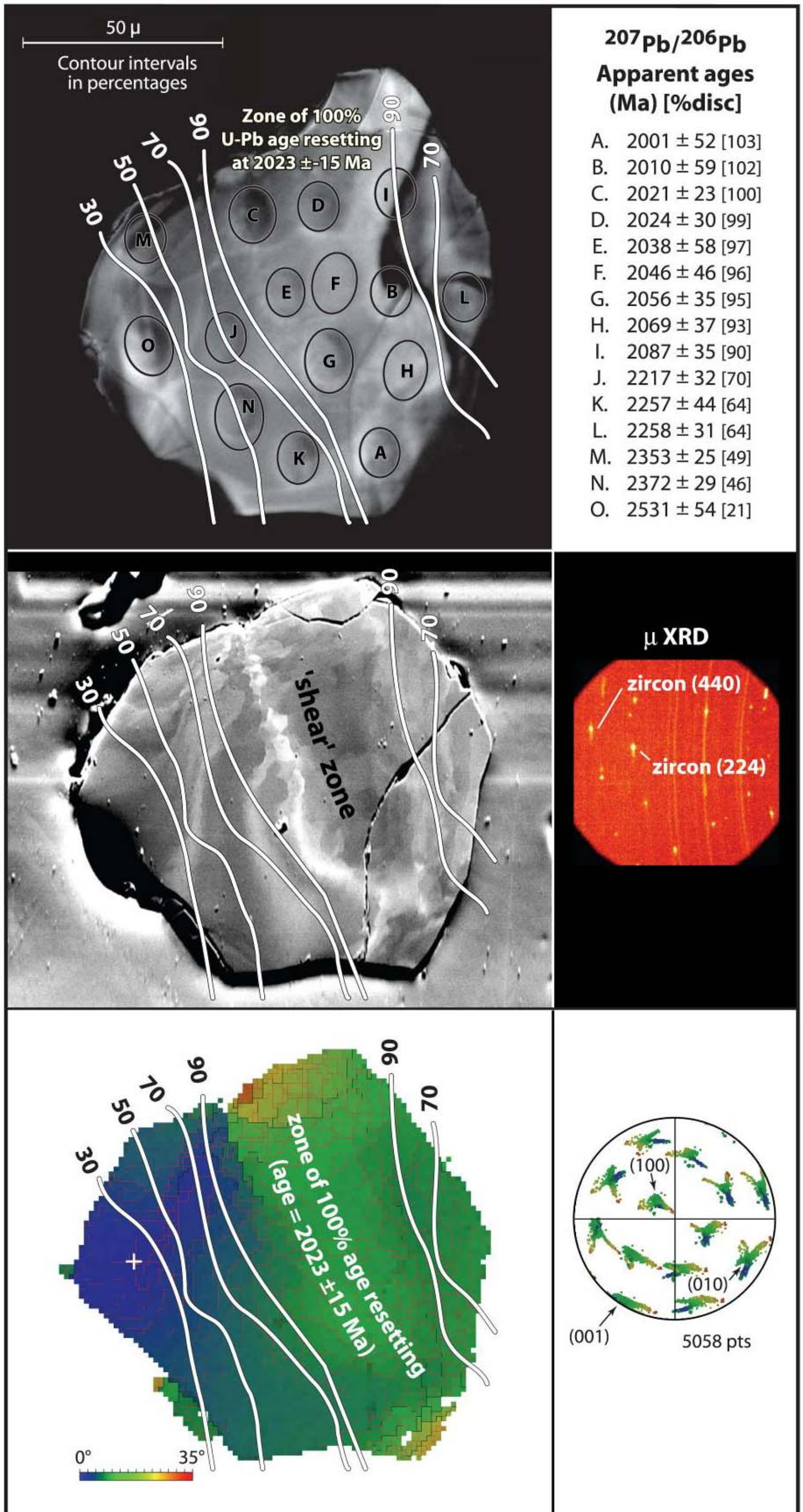

50 µ
Contour intervals in percentages
Zone of 100% U-Pb age resetting at 2023 ±-15 Ma
30
50
70
90
90
70
A
B
C
D
E
F
G
H
I
J
K
L
M
N
O
$^{207}Pb/^{206}Pb$ Apparent ages (Ma) [%disc]
A. 2001 ± 52 [103]
B. 2010 ± 59 [102]
C. 2021 ± 23 [100]
D. 2024 ± 30 [99]
E. 2038 ± 58 [97]
F. 2046 ± 46 [96]
G. 2056 ± 35 [95]
H. 2069 ± 37 [93]
I. 2087 ± 35 [90]
J. 2217 ± 32 [70]
K. 2257 ± 44 [64]
L. 2258 ± 31 [64]
M. 2353 ± 25 [49]
N. 2372 ± 29 [46]
O. 2531 ± 54 [21]
'shear' zone
µ XRD
zircon (440)
zircon (224)
zone of 100% age resetting (age = 2023 ±15 Ma)
0°
35°
(100)
(010)
(001)
5058 pts

Figure 5

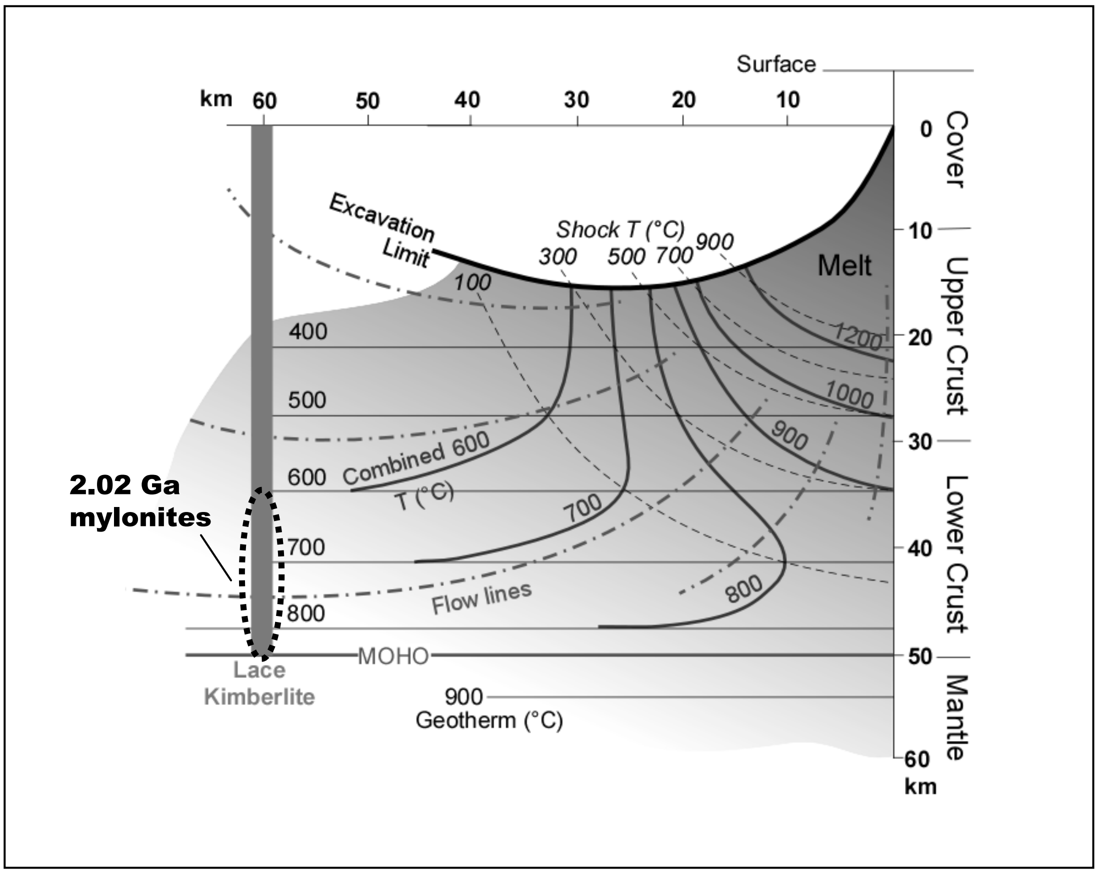

Fig. 5: Moser et al.